

# **$^{40}\text{Ar}/^{39}\text{Ar}$ and Rb-Sr Ages of the Tiegelongnan Porphyry Cu-(Au) Deposit in the Bangong Co-Nujiang Metallogenic Belt of Tibet, China: Implication for Generation of Super-Large Deposit**

LIN Bin<sup>1,2</sup>, CHEN Yuchuan<sup>1</sup>, TANG Juxing<sup>1,\*</sup>, WANG Qin<sup>3</sup>, SONG Yang<sup>1</sup>, YANG Chao<sup>4</sup>, WANG Wenlei<sup>5</sup>, HE Wen<sup>6</sup> and ZHANG Lejun<sup>2</sup>

1 *MLR Key Laboratory of Metallogeny and Mineral Assessment, Institute of Mineral Resources, Chinese Academy of Geological Sciences, Beijing 100037, China*

2 *Centre of Excellence in Ore Deposit (CODES), University of Tasmania, Hobart, 7001, Australia*

3 *Chengdu University of Technology, Chengdu 610059, China*

4 *Département de géologie et de génie géologique, Université Laval, Quebec, QC G1V0A6, Canada*

5 *Institute of Geomechanics, Chinese Academy of Geological Sciences, Beijing 100081, China*

6 *China University of Geosciences, Beijing 100083, China*

**Abstract:** The Tiegelongnan deposit is a newly discovered super-large porphyry-epithermal Cu-(Au) deposit in the western part of the Bangong Co-Nujiang metallogenic belt, Tibet (China). Field geology and geochronology indicate that the porphyry mineralization was closely related to the Early Cretaceous intermediate-felsic intrusions (ca. 123–120 Ma). Various epithermal ore and gangue mineral types were discovered in the middle-shallow part of the orebody, indicating the presence of epithermal mineralization at Tiegelongnan. Potassic, propylitic, phyllitic and advanced argillic alteration zones were identified.  $^{40}\text{Ar}/^{39}\text{Ar}$  dating of hydrothermal biotite (potassic zone), sericite (phyllitic zone), and alunite (advanced argillic zone) in/around the ore-bearing granodiorite porphyry yielded  $121.1 \pm 0.6$  Ma ( $1\sigma$ ),  $120.8 \pm 0.7$  Ma ( $1\sigma$ ) and  $117.9 \pm 1.6$  Ma ( $1\sigma$ ), respectively. Five hydrothermal mineralization stages were identified, of which the Stage IV pyrite was Rb-Sr dated to be  $117.5 \pm 1.8$  Ma ( $2\sigma$ ), representing the end of epithermal mineralization. Field geology and geochronology suggest that both the epithermal and porphyry mineralization belong to the same magmatic-hydrothermal system. The Tiegelongnan super-large Cu-(Au) deposit may have undergone a prolonged magmatic-hydrothermal evolution, with the major mineralization event occurring at ca. 120–117 Ma.

**Key words:**  $^{40}\text{Ar}/^{39}\text{Ar}$  and Rb-Sr dating, Tiegelongnan Cu-(Au) deposit, Bangong Co-Nujiang metallogenic belt, Tibet, Proto-Tethys

## 1 Introduction

Recent discoveries of Cu polymetallic mineralization in the western part of the Bangong Co-Nujiang suture (along the southern margin of the Qiangtang terrane and the northern margin of the Lhasa terrane) have led to the delineation of a large metallogenic belt, hereby named the Bangong Co-Nujiang metallogenic belt (BNMB) (Fig. 1) (Pan et al., 2012; Mao et al., 2014; Hou et al., 2015a, 2015b, 2015c; Huang et al., 2015; Zhu et al., 2015a; Sun et al., 2017). Previous studies showed that mineralization in the Bangong Co-Nujiang belt occurred in ca. 116–120 Ma

(Duolong ore cluster) and ca. 80–90 Ma (Gaerqiong-Galale ore cluster) (Li et al., 2014a, 2017; Zhang et al., 2015; Zhu et al., 2015b; Tang juxing et al., 2014b; Sun et al., 2017). Duolong is the largest ore cluster in the BNMB (Li et al., 2012a, 2012b, 2013, 2014a, 2017; Li yubin et al., 2012c; Lin et al., 2016), and more than four middle-large ( $\geq 50$  Mt of Cu ore) Cu-polymetallic deposits have been discovered, i.e., Duobuza (Li et al., 2011b, 2012b, 2013, 2014a, 2017), Bolong (Li et al., 2013, 2017), Naruo (Zhou et al., 2015) and the newly discovered Tiegelongnan (Tang juxing et al., 2014a, Fang xiang et al., 2015, Lin et al., 2017) (Fig. 2).

Geochemistry indicates that the ore-related intrusions in Duolong are mostly high-K calc-alkaline (Li et al., 2017,

\* Corresponding author. E-mail: tangjuxing@126.com

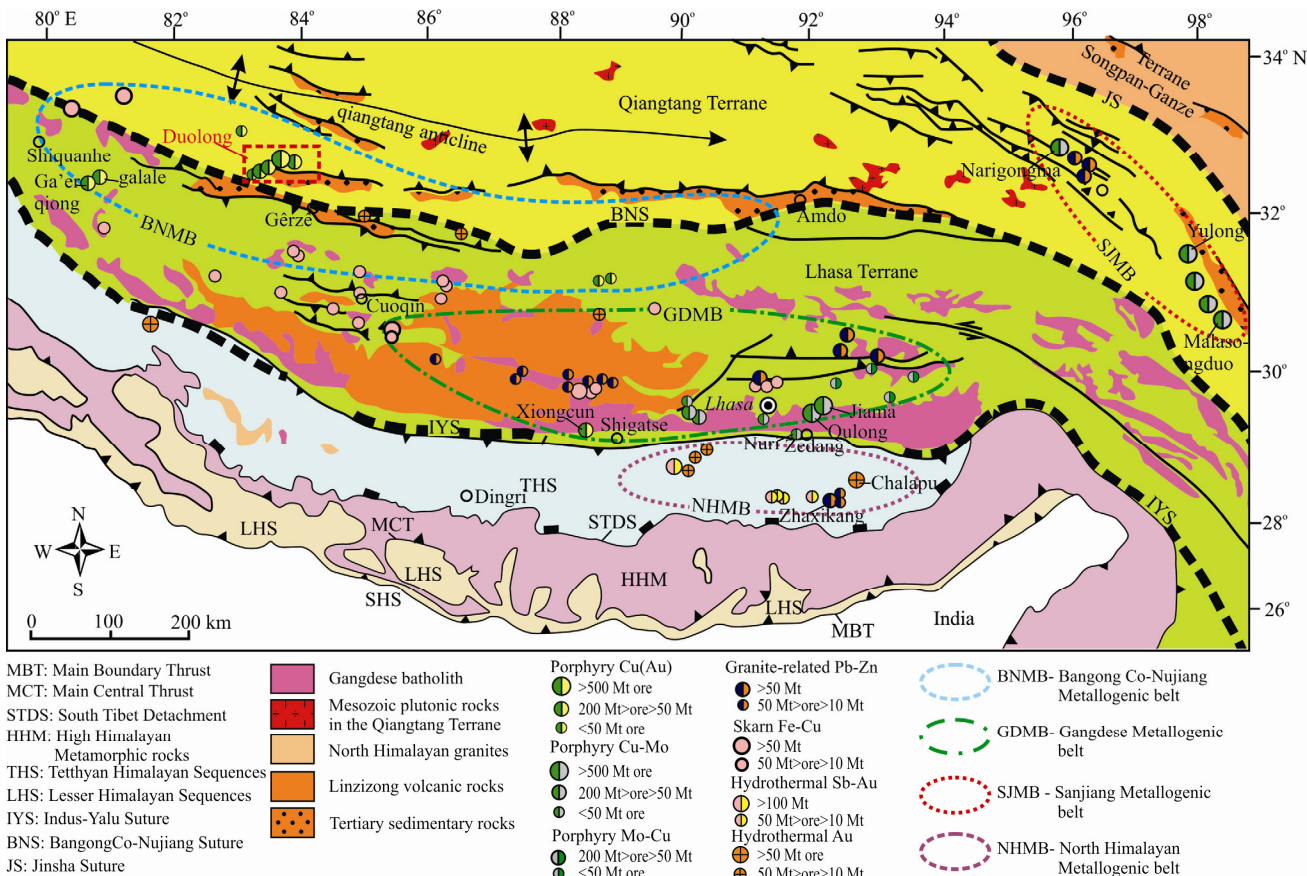


Fig. 1. Geological map of the Qinghai-Tibetan Plateau, showing the locations of the four major metallogenic belts and the Duolong ore district (after Yin et al., 2001; Hou et al., 2015).

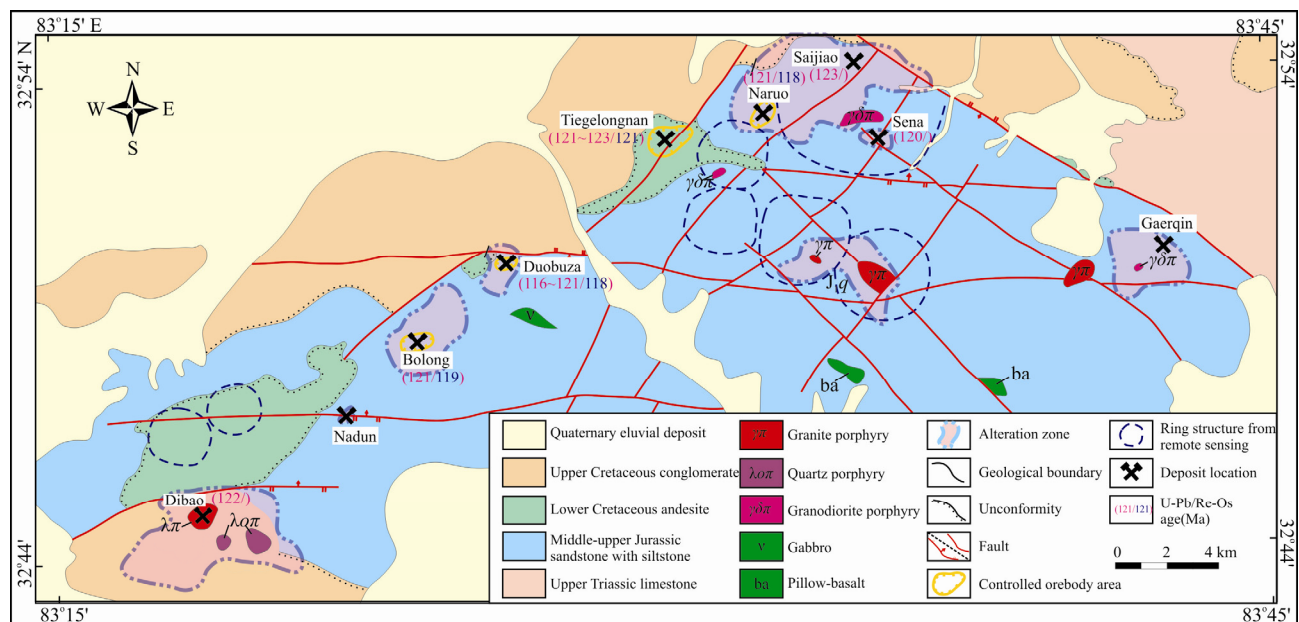


Fig. 2. Geological map of the Duolong ore district, showing the distribution of major Cu-(Au) deposits.

Zhu et al., 2015b) granodiorite porphyries and minor quartz diorite porphyries (Li et al., 2013; Lin et al., 2017). Their  $^{87}\text{Sr}/^{86}\text{Sr}_i$  values range from 0.7047 to 0.7090 and  $\varepsilon\text{Nd}(t)$  values range from -6.20 to 3.30 (Xin hongbo et al.,

2009, Li et al., 2013, 2014a, Chen Huaan et al., 2013, Sun jia, 2015, Zhu et al., 2015b), implying the mixture of lower crustal and mantle components (Li et al., 2013, Zhu et al., 2015b). Zircon U-Pb ages of the ore-bearing

porphyries in Duolong are mostly clustered around 120 Ma (Li et al., 2011b, 2012b, 2013, 2014a, 2017; Zhou et al., 2015; Fang Xiang et al., 2015; Lin et al., 2017), consistent with the mineralization (molybdenite Re-Os) ages ( $119.0 \pm 1.4$  Ma, Fang Xiang et al., 2015;  $121.2 \pm 1.2$  Ma, Lin et al., 2017).

Despite the numerous studies in the ore-bearing porphyries and the porphyry mineralization in Dulong, the epithermal mineralization there still remains poorly understood. The question concerned in the Dulong ore cluster is if there is any epithermal ores which is related to porphyry Cu system.

The Tiegelongnan Cu-(Au) deposit represents a good example to presence of both epithermal and porphyry mineralization. In this study, we aim to provide a coherent picture of how the Tiegelongnan super-large Cu-(Au) deposit was formed. We presented new data of mineralization and alteration, as well as pyrite Rb-Sr ages and  $^{40}\text{Ar}$ - $^{39}\text{Ar}$  ages of sericite, alunite and biotite to reveal the magmatic-hydrothermal evolution at Tiegelongnan.

## 2 Regional Geology

The Duolong ore cluster (DOC) in the Bangongco-Nujiang metallogenic belt (BNMB) is about 50 km long and 22 km wide (Song Yang et al., 2014). DOC is situated in the northern side of the Bangong Co-Nujiang suture and the southern margin of the Qiangtang terrane. The area consists mainly of Mesozoic pelagic sediments, some Cenozoic continental volcanics, conglomerates and sandstones. The Triassic Riganpeicuo Group, dominated by marble and limestone, is the oldest exposed unit in Duolong. The Riganpeicuo Group rocks are overlain by the Lower to Middle Jurassic Sewa Formation pelagic siltstone and sandstone. The rocks were previously interpreted to be bathyal to abyssal flysch (Li et al., 2013, 2014b), but are recently recognized as the metamorphosed accretionary complex that formed by the N-dipping subduction of the Bangong Co-Nujiang ocean basin (Li et al., 2011a; Yang Chao et al., 2014; Fang Xiang et al., 2015). The Jurassic Sewa Formation is overlain by the NE-trending fault-controlled Lower Cretaceous Meiriqiecuo Formation island-arc volcanics and minor volcaniclastics (Wang Qin et al., 2015; Sun Jia, 2015). The Meiriqiecuo Formation is overlain by the Upper Cretaceous Abushan Formation post-collisional molasses (conglomerate and sandstone) (Fig. 2).

Regional structures are well developed and control the igneous rock emplacement, and the mineralization-related ones are mainly NE-, EW- and NW-trending (Li et al., 2012b, 2013; Geng Quanru et al., 2011; Pan et al., 2012; Duan Zhiming et al., 2013). Except for the minor

occurrences of gabbro, diabase and pillow basalt in the Jurassic sedimentary sequences, regional magmatic rocks comprise mainly intermediate-felsic granitoids such as the Cu ore-hosting granodiorite/diorite/granite porphyries (She Hongquan et al., 2009; Zhu et al., 2015b; Zhou et al., 2015; Duan jilin et al., 2015). In addition, the Lower Cretaceous continental arc andesite, andesite porphyry and dacite form the immediate post-mineralization cover and are important for the Cu orebody preservation (Wang Qin et al., 2015; Lin et al., 2017).

## 3 Deposit Geology

The Tiegelongnan porphyry-epithermal Cu-(Au) deposit, located about 80 km NNW of Gêrzê County (Tibet), is the largest deposit in the DOC. Its total Cu ore resource is estimated to be over 2000 Mt @ 0.53 %. At Tiegelongnan, the Jurassic Sewa Formation ( $J_{1-2s}$ ) siltstone and sandstone is the oldest outcropping unit, which is overlain by the post-mineralized Meiriqiecuo Formation ( $K_1m$ ) andesite and dacite and then by the Abushan Formation ( $K_2a$ ) molasses (Figs. 1 and 2).

Field mapping and exploration drilling have identified the diorite porphyry (DP) and granodiorite porphyry (GDP) at Tiegelongnan to be Cu-(Au) ore-hosting (Lin et al., 2017). DP is only intersected as a small dyke in the drill cores, and does not have any direct contact relationship with GDP. It is difficult to identify the temporal relationship between GDP and DP. GDP contains mainly plagioclase (45–55%), quartz (25–30%), biotite (5–8%) and amphibole (15–20%) (Fig. 5g and h), while DP contains mainly plagioclase (55–75%) and amphibole (25–30%) and minor quartz (<5%). In addition, well-mineralized breccias were found deep in the GDP. The breccias contain sandstone clasts.

The biggest ore-body of the Tiegelongnan Cu-(Au) is roughly tubular- or funnel-shaped and are hosted in the ore-bearing GDP (Fig. 3b-c). Metallic minerals include mainly pyrite, chalcopyrite, molybdenite, digenite, bornite, covellite, enargite and hematite and minor azurite, malachite, limonite, sphalerite and galena (Fig. 4). Non-metallic minerals are predominately quartz, feldspar, biotite, sericite, chlorite, epidote, alunite, dickite and kaolinite, and minor calcite and anhydrite (Fig. 5a–e). Mineralization styles include disseminated, veinlet, breccia and stockwork (Fig. 5), exhibiting euhedral–subhedral and metasomatic-residual corrosion textures (Fig. 4a–d). Reflected light microscopy shows that the chalcopyrite is commonly xenomorphic, and molybdenite is commonly rosettes or flaky, whilst pyrite occurs mainly as metasomatic-residual grains and replaced by Cu sulfides (Fig. 4a).

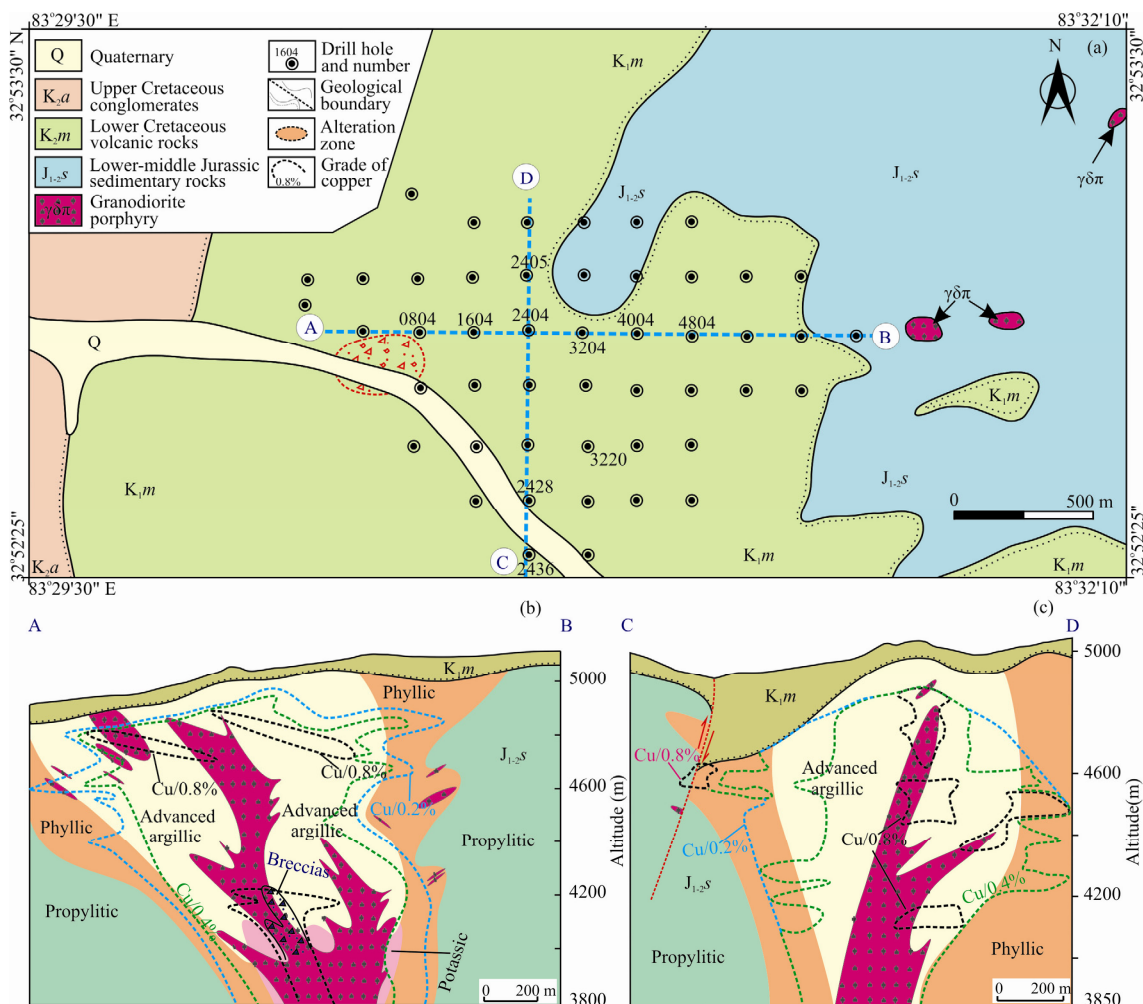


Fig. 3. Geologic map and cross sections of the Tiegelongnan deposit, Tibet.

Hydrothermal alteration is widespread at Tiegelongnan. Potassic, propylitic, phyllitic and advanced argillic alterations are present (Fig. 3b–c). Potassic alteration is the earliest alteration phase. It is represented by the abundant hydrothermal biotite, and occurs deep in the GDP and its surrounding rocks (Fig. 5e). In the GDP, some amphibole phenocrysts were replaced by hydrothermal biotite (Fig. 5g), and some hydrothermal biotite or biotite-quartz veins intruded the wall rocks. Disseminated and veinlet chalcopyrite, pyrite and molybdenite-quartz are present in this alteration zone. Potassic alteration was followed by propylitic alteration with abundant chlorite and epidote. Although much of the propylitic alteration was overprinted by the later phyllitic alteration, traces of propylitic alteration can still be found in the DP outside the mineralization center. In the propylitic alteration zone, chlorite and epidote occur as veinlets in the DP or pseudomorphs of plagioclase and amphibole, and the zone contains disseminated and veinlet chalcopyrite, pyrite and hematite. Phyllitic alteration is extensive at Tiegelongnan (Fig. 3b and c), and is featured

by disseminated secondary quartz and sericite after feldspars. Advanced argillic alteration is represented by the abundant kaolinite, dickite, alunite and vuggy quartz (Fig. 3b and c). Both phyllitic and advanced argillic alterations are spatially associated with the epithermal Cu-(Au) mineralization, dominated by disseminated bornite, digenite and enargite.

Based on hydrothermal/mineralization vein mineral assemblages and crosscutting relationships, five main hydrothermal/mineralization stages were recognized (Fig. 6): Stage I: Potassic alteration and chalcopyrite-pyrite-molybdenite mineralization; Stage II: Propylitic alteration and chalcopyrite-pyrite-hematite mineralization; Stage III: Phyllitic alteration and the subsequent advanced argillic alteration, accompanied by bornite-digenite-enargite mineralization. Stage IV: Pyrite veining and minor sphalerite-galena veining. Stage V: Supergene limonite-azurite-malachite mineralization. Stage I (porphyry) and III (epithermal) are the main hypogene mineralization stages.

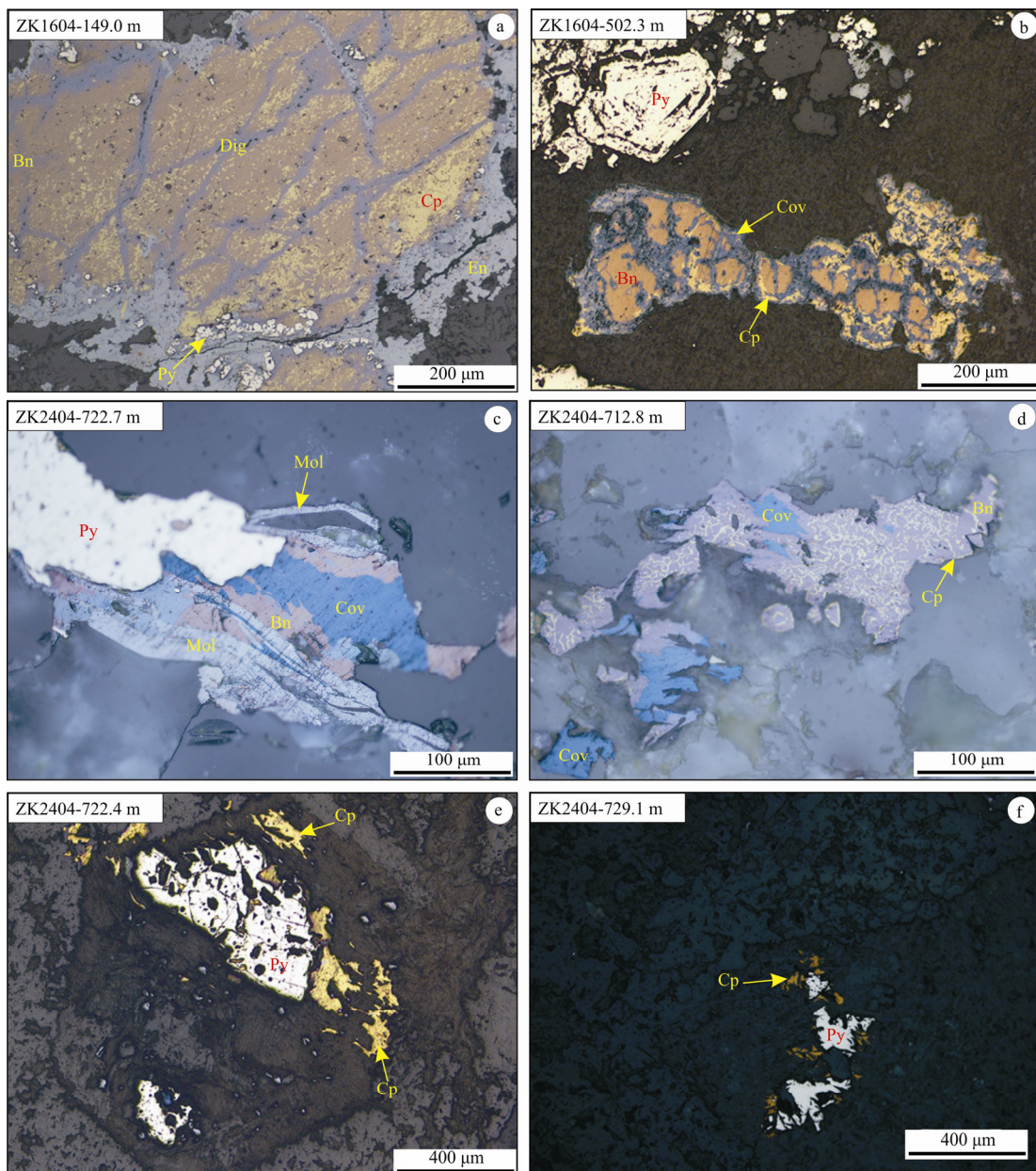


Fig. 4. Photomicrographs of typical ore minerals and textures of the Tiegelongnan deposit  
 (a) (ZK1604-149.0m) Dig, En, Bn partially replaced the Cp and Py; (b) (ZK1604-502.3m) Cov and Cp replaced Bn, with zoned pyrite; (c) (ZK2404-722.7m) Py, Mol and Bn replaced by Cov; (d) (ZK2404-712.8m) vermicular exsolution texture of Bn and Cp, both replaced by Cov; (e) (ZK2404-722.4m) Hb replaced by Py and Cp; (f) (ZK2404-729.1m) disseminated Cp and Py. Abbreviations: Dig-digenite; En-enargite; Py-pyrite; Cp-chalcopyrite; Bn-bornite; Mol-molybdenite; Cov-covellite; Hb-hornblende

## 4 Sampling and Analytical Methods

### 4.1 $^{40}\text{Ar}$ / $^{39}\text{Ar}$ dating

Hydrothermal biotite samples were collected from the deep potassic-altered wall rocks near the GDP (ZK4804, -1222.3 m deep), sericite samples were from the phyllitic-altered GDP (ZK2404, -737.7 m deep) and the alunite samples were from the advanced argillic-altered GDP (ZK1604, -383.7 m deep) (Fig. 7; Table 1). The samples were crushed and purified using a magnetic separator and then cleaned by ultrasonic treatment in ethanol. The purity

of the grains (0.08 to 0.15 mm) exceeded 99%. Samples were wrapped by aluminum foil and loaded into an aluminum tube, together with 2 or 3 monitor samples. The tubes were sealed into a quartz bottle (40 mm high; 50 mm in diameter) which were then irradiated for 51.75 hours in the Swimming Pool Nuclear Reactor at the Chinese Institute of Atomic Energy in Beijing with a neutron flux of  $\sim 6.4 \times 10^{12} \text{ n} \cdot \text{cm}^{-2} \cdot \text{s}^{-1}$ . The samples in the tube were irradiated by fast neutrons with an irradiation flux of  $1.16 \times 10^{18} \text{ n} \cdot \text{cm}^{-2}$ . After the irradiated samples cooled down enough to be safely handled, they were put into an

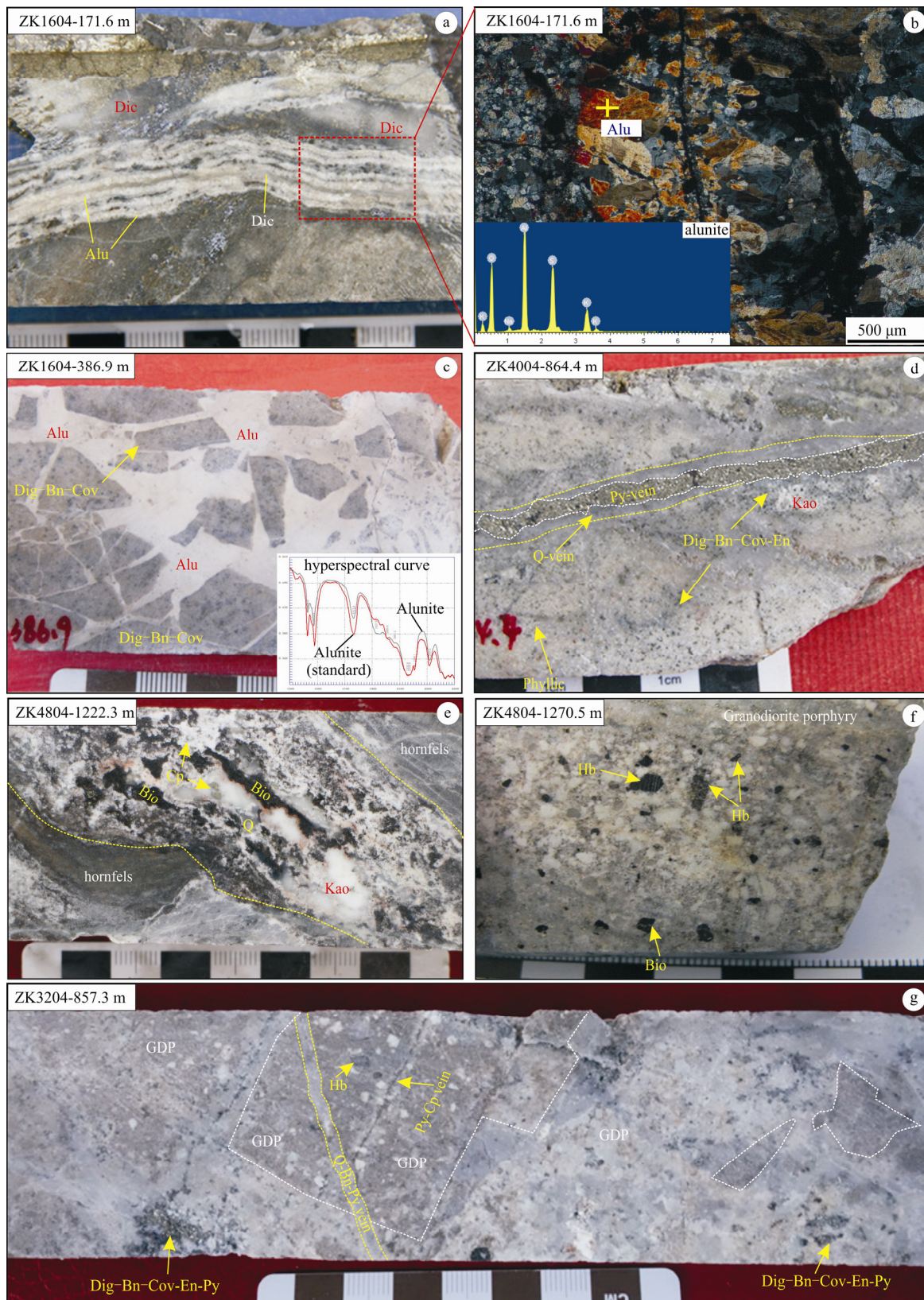


Fig. 5. Photos of typical alteration minerals and structures of the Tiegelongnan deposit  
(a) (ZK1604-171.6 m) banded Alu and Dic; (b) (ZK1604-171.6 m) microscopic picture and energy spectra of Alu; (c) (ZK1604-386.9 m) Alu cement in the Dig-Bn-Cov breccias and hyperspectral analysis of Alu (Stage III); (d) (ZK4004-864.4 m) late Py vein (Stage IV) crosscut Q vein in phyllitic altered rock, with minor disseminated Cov, En, Bn and Kao; (e) (ZK4804-1222.3 m) Bio, Kao, Q and Cp vein in hornfels; (f) (ZK4804-1270.5 m) disseminated Cp, Py in granodiorite porphyry; h: (ZK3204-857.3 m) granodiorite porphyry contain several sandstone clast. Abbreviations: Dig- digenite; En- enargite; Py- pyrite; Cp- chalcopyrite; Bn- bornite; Mol- molybdenite; Cov- covellite; Alu- alunite; Dic- dickite; Kao- kaolinite; Q- quartz; Hb- hornblende; Bio- biotite; SS- sandstone.

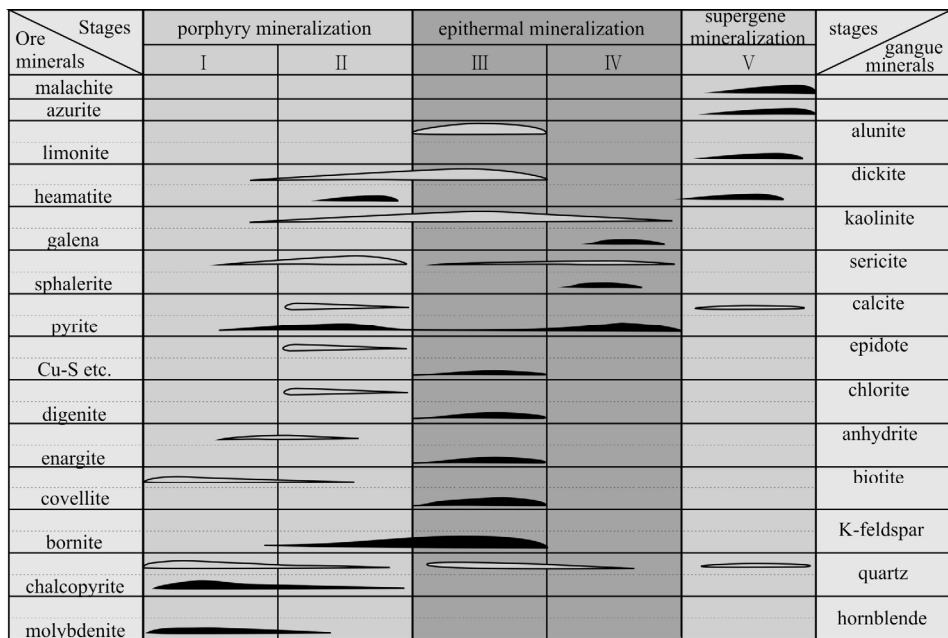


Fig. 6. Paragenetic sequence of ore and gangue minerals from the Tiegelongnan deposit and the three mineralization stages.

NB. the black and grey shapes represents the ore and gangue minerals, respectively.

**Table 1**  $^{40}\text{Ar}/^{39}\text{Ar}$  analytical data of biotite and alunite from the Tiegelongnan deposit

No. Step	T(°C)	$^{40}\text{Ar}/^{39}\text{Ar}$	$^{36}\text{Ar}/^{39}\text{Ar}$	$^{37}\text{Ar}/^{39}\text{Ar}$	$^{40}\text{Ar}^*/^{39}\text{Ar}_k$	$^{39}\text{Ar}(\% \text{ of cum})$	$^{40}\text{Ar}^*(\%)$	Age(Ma)	$\pm 1\sigma(\text{Ma})$
ZK4804-1222.3m biotite J=0.002742 W=30.1 mg									
1	800	26.9405	0.0060	0.0025	25.1613	22.04	93.40	121.48	0.62
2	850	25.2220	0.0008	0.0013	24.9809	19.33	99.04	120.64	0.60
3	900	25.1067	0.0005	0.0012	24.9523	14.63	99.38	120.50	0.60
4	950	25.1614	0.0006	0.0012	24.9859	6.04	99.30	120.66	0.60
5	1000	25.4488	0.0012	0.0016	25.0872	2.02	98.58	121.13	0.59
6	1050	25.5140	0.0012	0.0011	25.1479	1.44	98.57	121.42	0.60
7	1100	25.8099	0.0014	0.0028	25.3963	2.42	98.40	122.58	0.60
8	1200	25.3374	0.0008	0.0011	25.1041	20.98	99.08	121.21	0.60
9	1300	25.0904	0.0006	0.0010	24.9123	11.10	99.29	120.32	0.60
ZK1604-383.7 m alunite J=0.001505 W=24.9 mg									
1	550	175.8153	0.4199	0.0479	51.7553	0.01	29.44	137	20
2	600	61.2257	0.0577	0.0090	44.1745	0.17	72.15	117.2	2.2
3	650	46.4606	0.0085	0.0026	43.9523	7.06	94.60	116.6	1.2
4	700	46.0814	0.0055	0.0021	44.4465	16.93	96.45	117.9	1.2
5	750	45.9251	0.0046	0.0019	44.5659	13.79	97.04	118.2	1.2
6	800	49.5276	0.0146	0.0056	45.2273	0.16	91.32	119.9	1.5
7	900	101.9835	0.1873	0.1002	46.6423	0.02	45.73	123.5	9.8

ultra-high vacuum extraction and purification system made of stainless steel, whose vacuity is  $10^{-8}$  mm Hg. They were then baked for 48 hours at 120 to 150°C. The argon extraction system comprises an electron bombardment heated furnace in which the samples are heated under vacuum environment. A thermocouple was used to monitor and automatically control the temperature of the furnace. The furnace can automatically attain and maintain the setting temperature with variations of a few degrees. The released gases were admitted to a purification system. The heating-extraction step for each temperature increment and purification lasted 30 minutes. The purification system used a U-tube cooled with a mixture of acetone and dry ice, and a titanium sublimation pump with

38 Amp filament current and a titanium sponge furnace at 800°C. Finally, the gases were purified by two Sorb-AC pumps at room temperature. Purified argon was trapped in an activated charcoal finger at liquid-nitrogen temperature, and then released into the MM-1200 B Mass Spectrometer for the argon isotope analysis.

Measured isotopic ratios were corrected for mass discrimination, atmospheric argon component, blanks and irradiation-induced mass interference. The correction factors of interfering isotopes produced during irradiation were determined by analysis of irradiated pure  $\text{K}_2\text{SO}_4$  and  $\text{CaF}_2$ . Their values were:  $(^{36}\text{Ar}/^{37}\text{Ar})_{\text{Ca}} = 0.000240$ ;  $(^{40}\text{Ar}/^{39}\text{Ar})_k = 0.004782$ ; and  $(^{39}\text{Ar}/^{37}\text{Ar})_{\text{Ca}} = 0.000806$ . The blanks of  $m/e = 40, 39, 37, 36$  were below  $6 \times 10^{-15}$ , 4

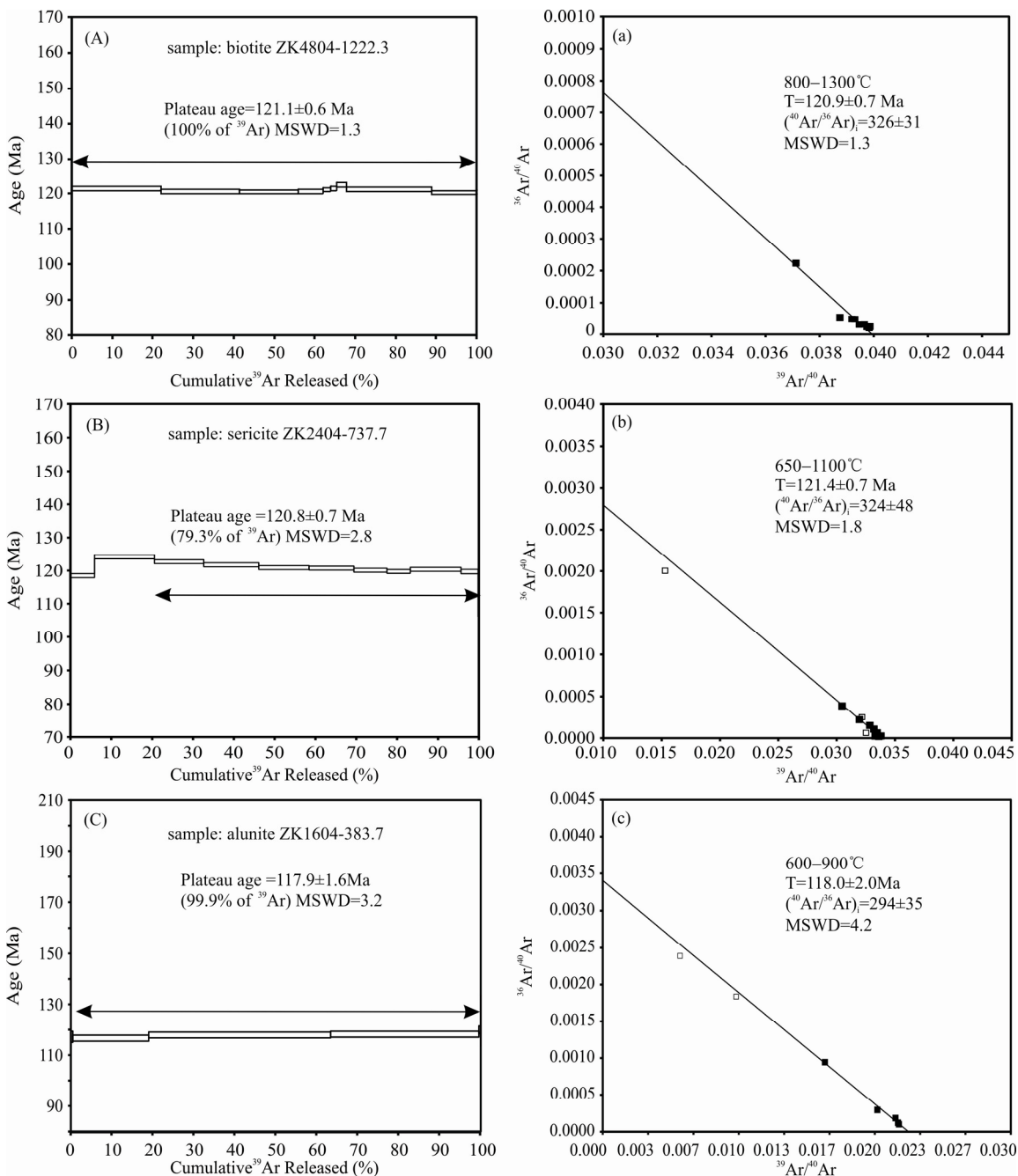


Fig. 7.  $^{40}\text{Ar}-^{39}\text{Ar}$  ages spectra, and isotope correlation diagrams of the biotite (A, a), sericite (B, b)(from Yang et al., in press ), alunite (C, c) in the Tiegelongnan deposit.

The plateau ages are indicated by the arrows. The solid square denotes the steps used in fitting invers isochron. 1 sigma is quoted for the points plotted in the isotope correlation diagrams.

$\times 10^{-16}$ ,  $8 \times 10^{-17}$  and  $2 \times 10^{-17}$  mol, respectively. The decay constant used was  $\lambda = 5.543 \times 10^{-10}$  /year (Steiger and Jäger, 1977). All  $^{37}\text{Ar}$  abundances were corrected for radiogenic decay (half-life 35.1 days). The uncertainty for each apparent age was given at one standard deviation. The Fangshan biotite (ZBH-25) was used as the internal standard, whose recommended age is  $132.7 \pm 1.2$  Ma and potassium content is  $7.579 \pm 0.030$  wt% (Wang sungshan, 1983). The  $^{40}\text{Ar}/^{36}\text{Ar}$  vs.  $^{39}\text{Ar}/^{36}\text{Ar}$  isochron diagram was

generated by using Isoplot (version 2.49) by Ludwig (2003). Details of the  $^{40}\text{Ar}/^{39}\text{Ar}$  dating procedures conducted were as described by Guo et al. (2011).

#### 4.2 Rb-Sr dating

Eight pyrite samples were from the undeformed Stage IV pyrite veins (Table 2), which represent the end of the epithermal mineralization.

The samples were rinsed several times with distilled

water, then dried and crushed to 40–60-mesh. Sphalerite and pyrite grains were handpicked under a binocular microscope, with purity reaching >98%. Sulfide grains were crushed to <200 mesh using an agate ball mill, then washed in an ultrasonic bath and dried. 0.2–0.3 gram of the sample powder was dissolved in Teflon beakers with a mixture of HF and HNO<sub>3</sub> acids. Rb–Sr was separated for isotope analysis using resin of AG50W×8 and different eluent reagents. First, REEs were separated from Rb–Sr by using cation-exchange chromatography with eluent of HCl, then Rb and Sr were separated using cation exchange column (Hu et al., 2015).

The Rb–Sr isotope analyses were performed using a VG 354 mass spectrometer with five collectors at the Center of Modern Analysis, Nanjing University. Details of the chemical separation and mass spectrometric procedures were described by Wang et al. (2007). <sup>87</sup>Sr/<sup>86</sup>Sr was normalized to <sup>86</sup>Sr/<sup>88</sup>Sr = 0.70806 ± 0.00010 to correct for the instrumental fractionation. Measurements for the American Standard Reference Material NBS 987 Sr standard yielded <sup>87</sup>Sr/<sup>86</sup>Sr = 0.710233±0.000006 (2σ). Regression and age calculations of isochrons were performed using Isoplot/Ex Version 3.0 software (Ludwig, 2003), with  $k = 1.42 \times 10^{-11} \text{ a}^{-1}$ . The errors for the <sup>87</sup>Rb/<sup>86</sup>Sr and <sup>87</sup>Sr/<sup>86</sup>Sr ratios at a confidence level of 95% were 1% and 0.005%, respectively.

## 5 Results

### 5.1 <sup>40</sup>Ar/<sup>39</sup>Ar dating

Previous studies have indicated that <sup>40</sup>Ar/<sup>39</sup>Ar dating of biotite, sericite and alunite can constrain the age of hydrothermal mineralization (Mao et al., 2006; Guo et al., 2011; Holly et al., 2016). The <sup>40</sup>Ar/<sup>39</sup>Ar analytical results are shown in Table 1 and Figure 7. In this study, the plateau ages were determined from seven or more continuous steps, comprising >75% of the total <sup>39</sup>Ar released, revealing concordant ages at the 95% confidence level (1σ).

The hydrothermal biotite (potassic alteration) yielded a well-defined plateau age of 121.1±0.6 Ma, slightly older than its inverse isochron age of 120.9±0.7 Ma (Fig. 7a). The initial <sup>40</sup>Ar/<sup>36</sup>Ar ratio (326.5±30.5), is broadly consistent with the atmospheric value (295.5) within analytical error.

Therefore, the biotite <sup>40</sup>Ar/<sup>39</sup>Ar age is reliable.

The altered sericite (ZK2404; phyllitic alteration) yielded a well-defined plateau age of 120.8±0.7 Ma, slightly younger than its inverse isochron age of 121.4±0.7 Ma (Fig. 7b). The initial <sup>40</sup>Ar/<sup>36</sup>Ar ratio (324.5±47) is broadly consistent with the atmospheric value (295.5) within analytical error. Therefore, the sericite <sup>40</sup>Ar/<sup>39</sup>Ar age is reliable.

The alunite (ZK1604; advanced argillic alteration) yielded a well-defined plateau age of 117.9±1.6 Ma, slightly younger than its inverse isochron age of 118.0±2.0 Ma (Fig. 7c). The initial <sup>40</sup>Ar/<sup>36</sup>Ar ratio of 294±35 is largely consistent with the atmospheric value (295.5) within the analytical error. Therefore, the alunite <sup>40</sup>Ar/<sup>39</sup>Ar age is reliable.

### 5.2 Rb-Sr dating

The Rb-Sr analytical data are listed in Table 2. The Rb (0.1027–0.8937 ppm) and Sr (0.2954–4.169 ppm) contents of the pyrite samples are relatively low, yielding <sup>87</sup>Rb/<sup>86</sup>Sr values of 0.0708 to 8.935. Meanwhile, the <sup>87</sup>Sr/<sup>86</sup>Sr values range widely from 0.708192 to 0.723053. The analytical data yielded an isochron age of 117.5±1.8 Ma with an initial <sup>87</sup>Sr/<sup>86</sup>Sr ratio of 0.70806±0.00010 (MSWD = 1.3) (Fig. 8).

## 6 Discussion

### 6.1 Temporal mineralization and alteration framework

Previous studies showed that the Tiegelongnan DP and GDP formation ages were ca. 123 Ma and 121 Ma, respectively (Fang et al., 2015; Lin et al., 2017), similar to the ore-hosting granitoids in other porphyry-related Cu-(Au) deposits in the DOC (Fig. 9), e.g., at Dibao (122.0 Ma), Nadun (117.9 Ma), Bolong (120.2–117.5 Ma), Duobuza (121.6–116.1 Ma), Naruo (125.0–120.2 Ma), Sena (122.0 Ma) and Saijiao (125.7 Ma) (Li et al., 2011b, 2012a, 2013, 2014b, 2015; Zhou et al., 2015a; Zhu et al., 2015b). These ages indicate a major porphyry-related Cu-(Au) metallogenic event at ca. 120 Ma in the DOC (Lin et al., 2017).

The published Re-Os molybdenite ages (119.0±1.4 Ma, Fang xiang et al., 2015; 121.2±1.2 Ma, Lin et al., 2017) are broadly coeval with the ore-hosting porphyry (zircon

**Table 2 Analytical data of Rb-Sr isotope ratios and Rb-Sr contents of Stage IV pyrites from the Tiegelongnan deposit.**

Sample	Mineral	Rb (ppm)	Sr (ppm)	<sup>87</sup> Rb/ <sup>86</sup> Sr	2σ	<sup>87</sup> Rb/ <sup>86</sup> Sr	2σ <sub>m</sub>
ZK2404-574.9	pyrite	0.2715	3.1750	0.2529	0.01	0.708514	0.00009
ZK2404-960.8	pyrite	0.1027	4.1690	0.0708	0.01	0.708192	0.00007
ZK2404-708.0	pyrite	0.3854	0.6276	1.8140	0.01	0.711258	0.00010
ZK2404-734.1	pyrite	0.3529	1.1280	0.9237	0.01	0.709503	0.00009
ZK2404-596.0	pyrite	0.5187	0.5265	2.9020	0.01	0.712946	0.00008
ZK2404-628.7	pyrite	0.7625	0.4393	5.1240	0.01	0.716532	0.00006
ZK2404-610.3	pyrite	0.8937	0.2954	8.9350	0.01	0.723053	0.00009
ZK2404-633.6	pyrite	0.6091	0.4727	3.8060	0.01	0.714284	0.00007

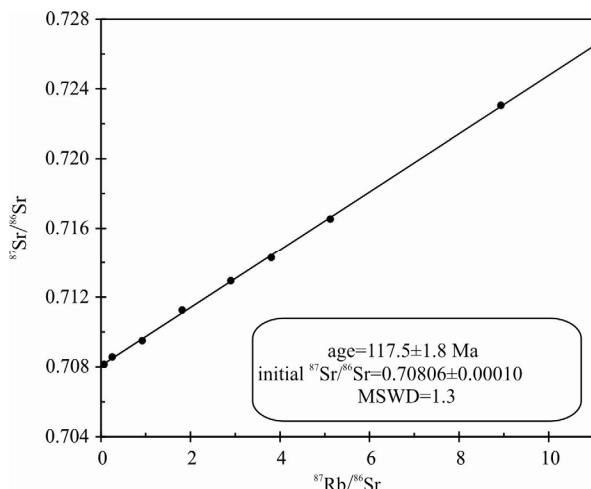


Fig. 8. Rb-Sr isochron ages of Stage IV pyrites from the Tiegelongnan deposit.

U-Pb age: ca. 123–121 Ma). Core logging indicates that the quartz-molybdenite veins were commonly crosscut by other sulfide veins and some molybdenite were replaced by other sulfides. Therefore, the Re-Os molybdenite ages constrain the timing of Stage I alteration, which marked the onset of porphyry mineralization (Fig. 10).

Our new pyrite Rb-Sr dating yielded 117.5±1.8 Ma. Core logging indicates that the pyrite veins are among the youngest and pyrite was not replaced by other minerals.

The Rb-Sr age of Stage IV pyrite thus constrain the end of epithermal mineralization to ca. 117 Ma (Fig. 10).

As for our new Ar-Ar ages for the hydrothermal biotite, sericite and alunite from Tiegelongnan, the potassic alteration (biotite  $^{40}\text{Ar}/^{39}\text{Ar}$  plateau age: 121.1±0.6 Ma) is coeval with the GDP emplacement (zircon U-Pb age: ca. 121 Ma) and porphyry Cu-(Au) mineralization (molybdenite Re-Os age: ca. 121 Ma). The close relationship between potassic alteration and porphyry mineralization is also evidenced by the occurrence of disseminated fine-grained chalcopyrite in hydrothermal biotite veins. The phyllitic alteration (sericite  $^{40}\text{Ar}/^{39}\text{Ar}$  plateau age: 120.8±0.7 Ma) is slightly younger than the potassic alteration, in accordance to classical porphyry ore deposit model (Cooke, 2005, Sillitoe, 2010). Alunite is a common indicator mineral of high-sulfidation epithermal mineralization (Deyell et al., 2005; Chang et al., 2011; King et al., 2014), and its Ar-Ar plateau age (117.9±1.6 Ma) shows that the advanced argillic alteration and high-sulfidation epithermal mineralization at Tiegelongnan are largely coeval with the pyrite mineralization (pyrite Rb-Sr age: 117.5 Ma) within analytical error.

## 6.2 Process of mineralization and duration of magmatic-hydrothermal system

It has been proposed that intensive and multi-stage

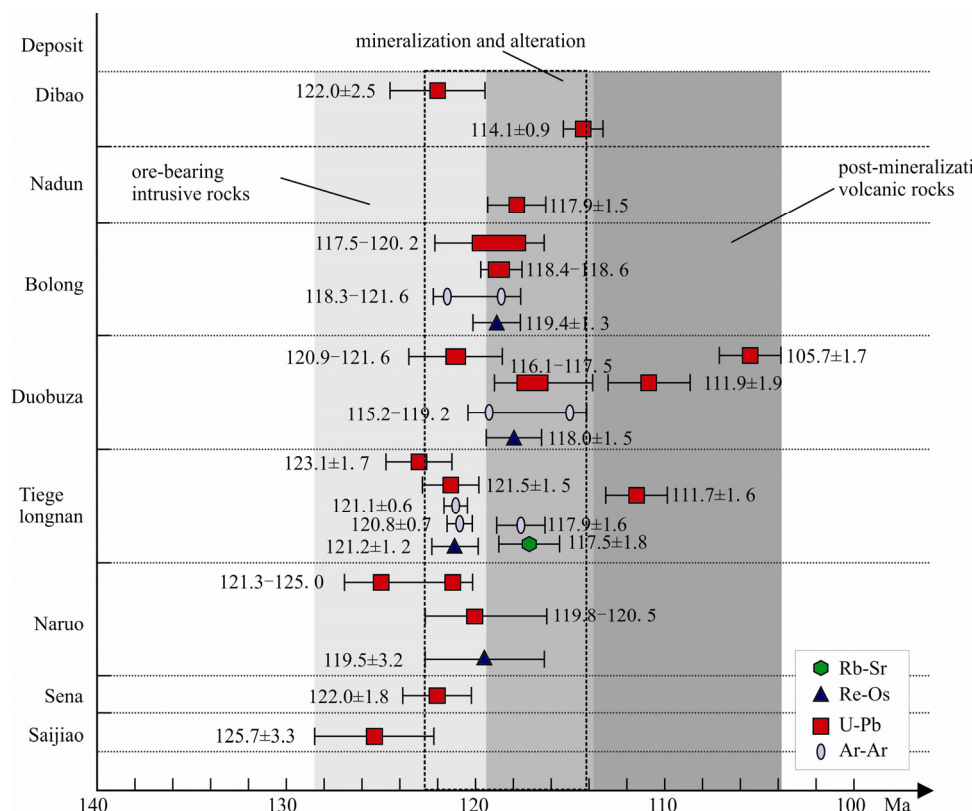


Fig. 9. Spatial-temporal framework of the magmatic evolution of the Duolong ore cluster.

Data are from Chen et al. (2013), Li et al. (2012b, 2012c, 2013, 2014a, 2014b), She et al. (2009), Sun (2015), Zhu et al. (2011, 2013, 2015b), Zhou et al. (2015), Duan et al. (2013), Fang et al. (2015) and Lin et al. (2016, 2017).

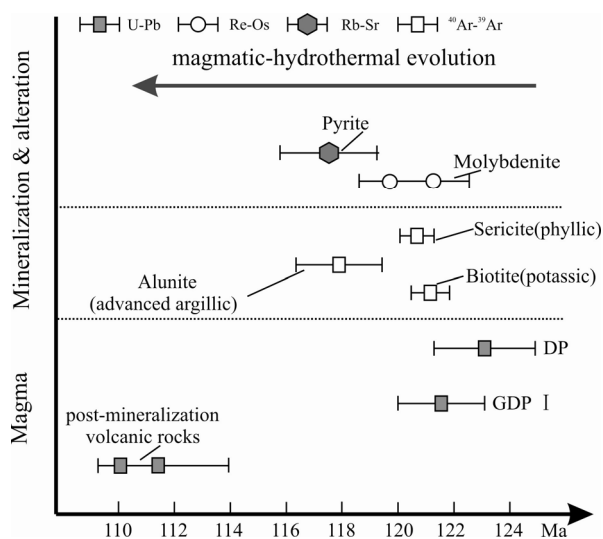


Fig. 10. Metallogenic spatial-temporal framework of the Tiegelongnan deposit.

Re-Os data from Fang et al. (2015) and Lin et al. (2017), DP and early GDP data from Lin et al. (2017), part of the volcanic rocks data from Wang et al. (2015).

magmatism occurred in the DOC (Li et al., 2013; Lin et al., 2017). At Tiegelongnan, the largest deposit in the DOC, the DP and GDP intruded the Jurassic sediments at ca. 123–121 Ma (zircon U-Pb). Moreover, our new  $^{40}\text{Ar}/^{39}\text{Ar}$  geochronology data suggest the ages of potassic, phyllitic and advanced argillic alterations are ca. 121.1 Ma, 120.8 Ma and 117.9 Ma, respectively. The Re-Os dating of Stage I molybdenite that represents the mineralization commencement yielded ca. 121–119 Ma, and the Rb-Sr dating of Stage IV pyrite that marks the end of mineralization yielded ca. 117.5 Ma.

All the molybdenite, biotite, sericite were from the deep GDP and its surrounding sandstones, and their ages are consistent with the zircon U-Pb age of GDP (121 Ma). It

is highly likely that the mineralization commencement (i.e., porphyry mineralization) and potassic alteration are closely related to the GDP emplacement. Both the pyrite and alunite were from the mineralized sandstone in shallow depth, and their occurrences represent the epithermal mineralization and the associated alteration. Their younger ages (ca. 117.5 Ma) than the potassic alteration and porphyry mineralization may reflect a relatively long-lived hydrothermal system.

We proposed that at Tiegelongnan, the DP and GDP may have intruded the Jurassic sediments at ca. 123–121 Ma, generating the potassic and propylitic alterations. At the same time, the GDP-derived ore-forming fluids may have percolated into and precipitated ore minerals in rock fissures and crystal cavities, forming porphyry-style disseminated and veinlet chalcopyrite, pyrite and molybdenite mineralization (ca. 121–119 Ma) (Fang xiang et al., 2015; Lin et al., 2017) (Fig. 11a). Later on, the ascending magmatic-dominated hydrothermal fluids may have mixed with meteoric water at shallow crustal level to produce extensive phyllitic and advanced argillic alteration and high-sulfidation epithermal mineralization (Fig. 11b). The Tiegelongnan deposit was then exhumed during the Late Cretaceous uplifting of the South Qiangtang terrane. Post-mineralization andesitic volcanics (110 Ma) has helped preserve the Tiegelongnan deposit from further erosion (Fig. 11c). We conclude that the epithermal and porphyry mineralization at Tiegelongnan are genetically linked and belong to the same magmatic-hydrothermal system.

Li et al. (2013) and Yang zhiming et al. (2008) suggested that many super-large porphyry Cu-(Au) deposits have undergone prolonged magmatic-hydrothermal activities (Huang et al., 2017), such as the Duobza (about 3–4 m.y.) and Qulong porphyry deposits (about 6 m.y.) in Tibet. To determine the lifespan of a multi-stage porphyry system,

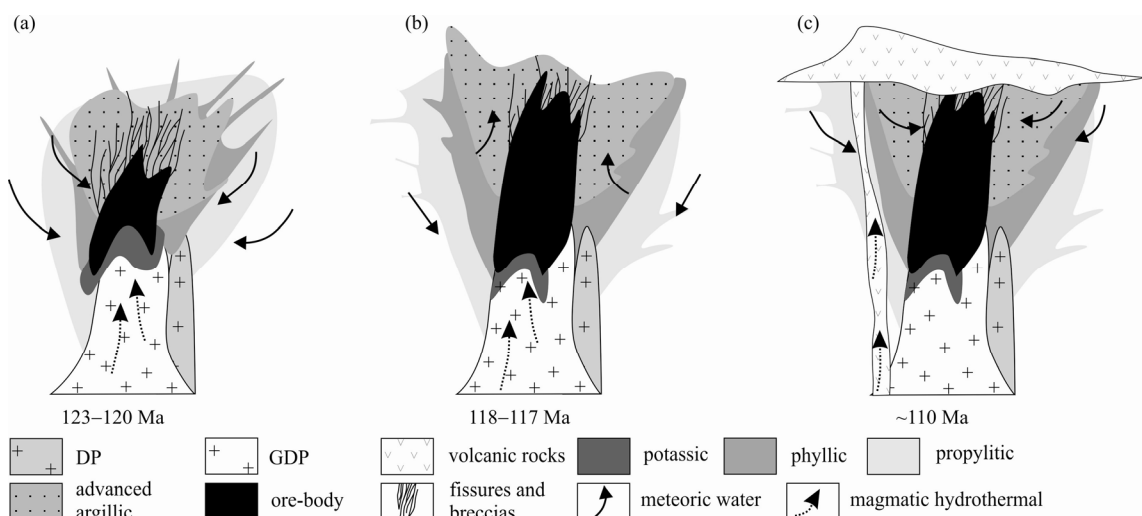


Fig. 11. Schematic metallogenic model of the Tiegelongnan deposit.

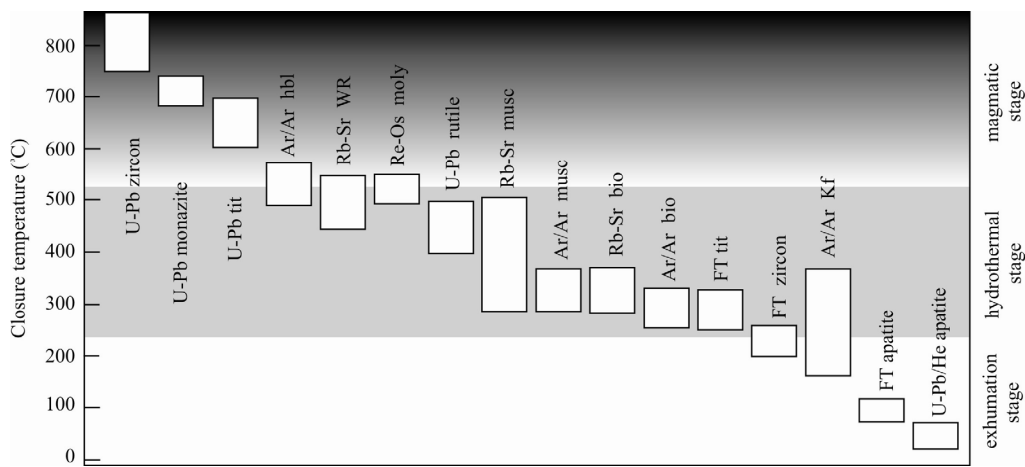


Fig. 12. Range of closure temperatures of different geochronometers (from Chiaradia et al., 2013).

zircon U-Pb ages record the upper temperature limit of porphyry systems because of the high closure temperature ( $\sim 900^{\circ}\text{C}$ ) (Fig. 12). Closure temperatures of Re-Os in molybdenite are about  $500 \sim 600^{\circ}\text{C}$  (Fig. 12) (Chiaradia et al., 2013), and thus molybdenite Re-Os dating can record the age of the porphyry mineralization.  $^{40}\text{Ar}/^{39}\text{Ar}$  dating of K-bearing minerals (biotite, sericite and alunite) often represents the age when the hydrothermal system cooled below  $300^{\circ}\text{C}$  (closure temperatures of K-Ar isotope system).  $^{40}\text{Ar}/^{39}\text{Ar}$  ages of biotite and sericite both suggest that the potassic and phyllitic alterations ended at ca. 121–120 Ma, consistent with the molybdenite Re-Os and zircon U-Pb age of the GDP.  $^{40}\text{Ar}/^{39}\text{Ar}$  age of alunite and Rb-Sr age of pyrite (ca. 118–117 Ma) represent the slightly younger epithermal mineralization. This indicates that the duration of magmatic-hydrothermal event at Tiegelongnan was about 2–4 m.y. Given the analysis error, geochronology study in Tiegelongnan still suggests that prolonged magmatic-hydrothermal activity is helpful for the large-scale mineralization.

## 7 Conclusions

(1) Potassic, propylitic, phyllitic and argillic alterations were identified at Tiegelongnan.  $^{40}\text{Ar}/^{39}\text{Ar}$  ages of hydrothermal biotite ( $121.1 \pm 0.6$  Ma), sericite ( $120.8 \pm 0.7$  Ma) and alunite ( $117.9 \pm 1.6$  Ma) were interpreted to represent the timing of potassic, phyllitic and advanced argillic alteration, respectively.

(2) Five hydrothermal stages were identified. Rb-Sr age of Stage IV pyrite ( $117.5 \pm 1.8$  Ma) was interpreted to represent the end of mineralization.

(3) The epithermal and porphyry mineralization at Tiegelongnan were closely related, with both resulting from the same prolonged magmatic-hydrothermal event at ca. 120–117 Ma.

## Acknowledgments

We are grateful to two anonymous reviewers and the Editor-in-Chief for their constructive comments. This work was jointly sponsored by the Public Science and Technology Research Funds Projects, Ministry of Land Resources of the People's Republic of China (project No. 201511017 and 201511022-02); the Basic Research Fund of the Chinese Academy of Geological Sciences (Grant No. YYWF201608); the National Natural Science Foundation of China (Grant No. 41402178); Geological Survey Project of the China Geological Survey (project 1212011405040), Golden Dragon Mining Co. Ltd. (project XZJL-2013-JS03) and China Scholarship Council. Cenozoic Geoscience Editing & Consultancy (Australia) is acknowledged for its scientific and language editing service.

Manuscript received May 23, 2016

accepted Jan. 18, 2017

edited by Fei Hongcai

## References

- Chang, Z.S., Hedenquist, J.W., White, N.C., Cooke D.R., Roach, M., Deyell, C.L., Joey, G.J., Gemmell, B., McKnight S., and Cuson, A.L., 2011. Exploration tools for linked porphyry and epithermal deposits: example from the Mankayan intrusion-centered Cu-Au District, Luzon, Philippines. *Economic Geology*, 106(8): 1365–1398.
- Chen Huaan, Zhu Xiangping, Ma Dongfang, Huang Hanxiao, Li Guangming, Li Yubin, Li Yuchuang, Wei Lujie and Liu Chaoqiang, 2013. Geochronology and geochemistry of the Bolong porphyry Cu-Au deposit, Tibet and its mineralizing significance. *Acta Geologica Sinica*, 87: 1593–1611 (in Chinese with English abstract).
- Chiaradia, M., Schaltegger, U., Spikings, R., Wotzlaw, J.F., and Ovtcharova, M., 2013. How accurately can we date the duration of magmatic-hydrothermal events in porphyry

- systems?—an invited paper. *Economic Geology*, 108(4): 565–584.
- Cooke, D.R., Hollings, P., and Walshe, J.L., 2005. Giant-porphyry-deposits: characteristics, distribution, and tectonic Controls. *Economic Geology* 100: 801–818.
- Deyell, C.L., Leonardson, R., Rye, R.O., Thompson, J.F.H., Bissig, T., and Cooke, D.R., 2005. Alunite in the Pascua-Lama high-sulfidation deposit: constraints on alteration and ore deposition using stable isotope geochemistry. *Economic Geology*, 100(1): 131–148.
- Duan Jilin., Tang Juxing, Li Yubin., Liu Shengao, Wang Qin, Yang Chao and Wang Yiyun, 2015. Copper isotopic signature of the Tiegelongnan high-sulfidation copper deposit, Tibet: implications for its origin and mineral exploration. *Mineralium Deposita*, 1–12.
- Duan Zhiming, Li Guangming, Zhang Hui, Li Yingxu and Duan Yaoyao, 2013. Zircon U-Pb age and geochemical characteristics of the quartz monzobiorite and metallogenic background of the Sena gold deposit in Duolong metallogenic concentrated area, Tibet. *Journal of Jilin University (Earth Science Edition)*. 43: 1864–1877 (in Chinese with English abstract).
- Fang Xiang, Tang Juxing, Song Yang, Yang Chao, Ding Shuai, Wang Yiyun, Wang Qin, Sun Xinguo, Li Yubin, Wei Lujie, Zhang Zhi, Yang Huanhuan, Gao ke and Tang Pan, 2015. Formation epoch of the south Tiegelong super-large epithermal Cu (Au-Ag) deposit in Tibet and its geological implications. *Acta Geoscientica Sinica*, 36(2): 168–176 (in Chinese with English abstract).
- Gen Quanru, Pan Guitang, Wang Liquang, Peng Zhimin and Zhang Zhang, 2011. Tethyan evolution and metallogenic geological background of the Bangong co-Nujiang belt and the Qiangtang massif in Tibet. *Geological Bulletin of China*, 30: 1261–1274 (in Chinese with English abstract).
- Guo Chunli, Mao Jingwen, Bierlein, F., Chen Zhenghui, Chen Yuchuan, Li Chuanbiao and Zeng Zailin, 2011. SHRIMP U-Pb (zircon), Ar-Ar (muscovite) and Re-Os (molybdenite) isotopic dating of the Taoxikeng tungsten deposit, South China Block. *Ore Geology Reviews*, 43(1): 26–39.
- Holley, E.A., Bissig, T., and Monecke, T., 2016. The Veladero high-sulfidation epithermal gold deposit, El Indio-Pascua belt, Argentina: geochronology of alunite and jarosite. *Economic Geology*, 111(2): 311–330.
- Hou Zengqian, Duan Lianfeng, Lu Yongjun, Zheng Yuanchuan, Zhu Dichen, Yang Zhiming, Yang Zhusen, Wang Baodi, Pei Yingru, Zhao Zhidan and McCaig, T.C, 2015a. Lithospheric architecture of the Lhasa terrane and its control on ore deposits in the Himalayan-Tibetan orogen. *Economic Geology*, 110(6): 1541–1575.
- Hou Zengqian, Yang Zhiming, Lu Yongjun, Kemp, A., Zheng Yuanchuan, Li Qiuyun, Tang Juxing, Yang Zhusen and Duan Lianfeng, 2015b. A genetic linkage between subduction- and collision-related porphyry Cu deposits in continental collision zones. *Geology*, 43(3): 247–250.
- Hou, Zengqian, Zhang, Hongrui, 2015c. Geodynamics and metallogeny of the eastern Tethyan metallogenic domain. *Ore Geology Reviews*, 70: 346–384.
- Hu Qiaoqing, Wang Yitian, Mao Jingwen, Wei Ran, Liu Shengyou, Ye Dejin, Yuan Qunhu and Dou Ping, 2015. Timing of the formation of the Changba-Lijiagou Pb-Zn ore deposit, Gansu Province, China: Evidence from Rb-Sr isotopic dating of sulfides. *Journal of Asian Earth Sciences*, 103: 350–359.
- Huang Qishuai, Shi Rendeng, O'Reilly, S.Y., Griffin, W.L., Zhang Ming, Liu Deliang and Zhang Xiaoran, 2015. Re-Os isotopic constraints on the evolution of the Bangong-Nujiang Tethyan oceanic mantle, Central Tibet. *Lithos*, 224–225: 32–45.
- Huang Yong, Li Guangming, Ding Jun, Dai Jie, Yan Guoqiang, Dong Suiliang, Huang Hanxiao, 2017. Origin of the newly discovered Zhunuo porphyry Cu-Mo-Au deposit in the western part of the Gangdese porphyry copper belt in the southern Tibetan Plateau, SW China. *Acta Geologica Sinica (English Edition)*, 91(1): 109–134.
- King, J., Williams-Jones, A.E., van Hinsberg, V., and Williams-Jones, G., 2014. High-sulfidation epithermal pyrite-hosted Au (Ag-Cu) ore formation by condensed magmatic vapors on Sangihe island, Indonesia. *Economic Geology*, 109(6): 1705–1733.
- Li Guangming, Duan Zhiming, Liu Bo, Zhang Hui, Dong Suiliang and Zhang Li, 2011a. The discovery of Jurassic accretionary complexes in Duolong area,northern Bangong Co-Nujiang suture zone, Tibet, and its geologic significance. *Geological Bulletin of China*, (08): 1256–1260 (in Chinese with English abstract).
- Li Guangming, Qin Kezhang, Li Jinxiang, Evans, N.J., Zhao Junxing, Cao Mingjian and Zhang Xianan, 2017. Cretaceous magmatism and metallogeny in the Bangong-Nujiang metallogenic belt, central Tibet: Evidence from petrogeochemistry, zircon U-Pb ages, and Hf-O isotopic compositions. *Gondwana Research*, 110–127.
- Li Guangming, Zhang Xianan, Qin Kezhang, Sun Xinguo, Zhao Junxing, Yin Xianbo, Li Jinxiang and Yuan Huashan, 2015. The telescoped porphyry-high sulfidation epithermal Cu (-Au) mineralization of Rongna deposit in Duolong ore cluster at the southern margin of Qiangtang Terane, Central Tibet: Integrated evidence from geology, hydrothermal alteration and sulfide assemblages. *Acta Petrologica Sinica*, (08): 2307–2324 (in Chinese with English abstract).
- Li Guangming, Li Jinxiang, Qin Kezhang, Duo Ji, Zhang Tianping, Xiao Bo and Zhao Junxing, 2012a. Geology and hydrothermal alteration of the Duobuzha gold-rich porphyry copper district in the Bangongco metallogenic belt, northwestern Tibet. *Resource Geology*, 62(1): 99–118.
- Li Jinxiang, Qin Kezhang, Li Guangming, Richards, J.P., Zhao Junxing and Cao Mingjian, 2014a. Geochronology, geochemistry, and zircon Hf isotopic compositions of Mesozoic intermediate-felsic intrusions in central Tibet: Petrogenetic and tectonic implications. *Lithos*, 198–199: 77–91.
- Li Jinxiang, Qin Kezhang, Li Guangming, Xiao Bo, Zhao Junxing, Cao Mingjian and Chen Lei, 2013. Petrogenesis of ore-bearing porphyries from the Duolong porphyry Cu–Au deposit, central Tibet: Evidence from U-Pb geochronology, petrochemistry and Sr-Nd-Hf-O isotope characteristics. *Lithos*, 160–161: 216–227.
- Li Jinxiang, Qin Kezhang, Li Guangming, Xiao Bo, Zhao Junxing and Chen Lei, 2014b. Petrogenesis of Cretaceous igneous rocks from the Duolong porphyry Cu–Au deposit, central Tibet evidence from zircon U-Pb geochronology, petrochemistry and Sr-Nd-Pb-Hf isotope characteristics. *Geological Journal*, DOI: 10.1002/gj.2631

- Li Jinxiang, Li Guangming, Qin Kezhang, Xiao Bo, Chen Lei and Zhao Junxing, 2012b. Mineralogy and mineral chemistry of the cretaceous Duolong gold-rich porphyry copper deposit in the Bangongco arc, northern Tibet. *Resource Geology*, 62 (1): 19–41.
- Li Jinxiang, Qin Kezhang, Li Guangming, Xiao Bo, Zhang Junxing and Chen Lei, 2011b. Magmatic-hydrothermal evolution of the Cretaceous Duolong gold-rich porphyry copper deposit in the Bangongco metallogenic belt, Tibet: Evidence from U-Pb and  $^{40}\text{Ar}/\text{Ar}$  geochronology. *Journal of Asian Earth Sciences*, 41(6): 525–536.
- Li Shimin, Zhu Dicheng, Wang Qing, Zhao Zhidan, Sui Qinglin, Liu Sheng'ao and Liu Dong, 2014c. Northward subduction of Bangong–Nujiang Tethys: Insight from Late Jurassic intrusive rocks from Bangong Tso in western Tibet. *Lithos*, 205: 284–297.
- Li Yubin, Duo Ji, Zhong Wanting, Li Yuchang, Qiangba Wangdui, Chen Hongqi, Liu Hongfei, Zhang Jinshu, Zhang Tianping, Xu Zhizhong, Fan Anhui and Suolang Wangqin, 2012c. An exploration model of the Duobuza porphyry Cu-Au deposit in Gaize country, northern Tibet. *Geology and Prospecting*, (02): 274–287 (in Chinese with English abstract).
- Lin Bin, Chen Yuchuan, Tang Juxing, Song Yang, Wang Qin, Feng Jun, Li Yanbo, Tang Xiaoqian, Lin Xin, Liu Zhibo, Wang Yiyun, Fang Xiang, Yang Chao, Yang Huanhuan, Fei Fan, Li Li and Gao Ke, 2016. Zircon U-Pb Ages and Hf Isotopic Composition of the Ore-bearing Porphyry in Dibao Cu(Au)Deposit,Duolong Ore Concentration Area,Xizang (Tibet),and Its Geological Significance. *Geological Review*, 62(6): 1564–1678 (in Chinese with English abstract).
- Lin Bin, Tang Juxing, Chen Yuchuan, Song Yang., Greg Hall, Wang Qin., Yang Chao, Fang Xiang, Duan Jilin, Yang Huanhuan, Liu Zhibo, Wang Yiyun and Feng Jun, 2017. Geochronology and genesis of the Tiegelongnan porphyry Cu (Au) deposit in Tibet: evidence from U-Pb, Re-Os dating and Hf, S, and H-O isotopes. *Resource Geology*, 67(1): 1–21.
- Ludwig, K.R., 2003. User's manual for Isoplot 3.00: A *Geochronological Toolkit for Microsoft Excel*, 4. Berkeley Geochronology Center Special Publication.
- Mao Jingwen, Wang Yitian, Lehmann, B., Yu Jinjie, Du Andao, Mei Yanxiong, Li Yongfeng, Zang Wenshuan, Stein, H.J., and Zhou Taofa, 2006. Molybdenite Re-Os and albite Ar-40/Ar-39 dating of Cu-Au-Mo and magnetite porphyry systems in the Yangtze River valley and metallogenic implications. *Ore Geology Reviews*, 29(3–4): 307–324.
- Mao Jingwen, Pirajno, F., Lehmann, B., Luo Maocheng and Berzina A., 2014. Distribution of porphyry deposits in the Eurasian continent and their corresponding tectonic settings. *Journal of Asian Earth Sciences*, 79: 576–584.
- Pan Guitang, Wang, Liquan, Li, Rongshe, Yuan Sihua, Ji Wenhua, Yin Fuguang, Zhang Wanping and Wang Baodi, 2012. Tectonic evolution of the Qinghai-Tibet Plateau. *Journal of Asian Earth Sciences*, 53: 3–14.
- She Hongquan, Li Jinwen, Ma Dongfang, Li Guangming, Zhang Dequan, Feng Chengyou, Qu Wenjun and Pan Guitang, 2009. Molybdenite Re-Os and SHRIMP zircon U-Pb dating of Duobuza porphyry copper deposit in Tibet and its geological implications. *Mineral Deposits*, 28: 737–746 (in Chinese with English abstract).
- Sillitoe, R.H., 2010. Porphyry Copper Systems. *Economic Geology*, 105(1): 3–41.
- Song Yang, Tang Juxing, Qu Xiaoming, Wang Denghong, Xin Hongbo, Yang Chao, Lin Bin and Fan Shufang, 2014. Progress in the study of mineralization in the Bangongco-Nujiang metallogenic belt and some new recognition. *Advances in Earth Science*. (07): 795–809 (in Chinese with English abstract).
- Steiger, R.H., and Jäger, E., 1977. Subcommission on geochronology: Convention on the use of decay constants in geo- and cosmo-chronology. *Earth Planet Sci Lett* 36: 359–362.
- Sun Jia, 2015 *Magmatism and metallogenesis at Duolong ore district, Tibet*. (Doctoral dissertation), China University of Geosciences, Beijing (in Chinese with English abstract).
- Sun Jia, Mao Jingwen, Beaudoin, G., Duan Xianzhe, Yao Fojun, Ouyang Hegen, Wu Yue, Li Yubin and Meng Xuyang. 2017. Geochronology and geochemistry of porphyritic intrusions in the Duolong porphyry and epithermal Cu-Au district, central Tibet: implications for the genesis and exploration of porphyry copper deposits. *Ore Geology Reviews*, 80: 1004–1019.
- Tang Junxing, Sun Xinguo, Ding Shuai, Wang Qin, Wang Yiyun, Yang Chao, Chen Hongqi, Li Yanbo, Li Yubin, Wei Lujie, Zhang Zhi, Song Junlong, Yang Huanhuan, Duan Jilin, Gao Ke, Fang Xiang and Tan Jiangyun, 2014a. Discovery of the epithermal deposit of Cu (Au-Ag) in the Duolong ore concentrating area, Tibet. *Acta Geoscientia Sinica*, 35: 6–10 (in Chinese with English abstract).
- Tang Juxing, Wang Qin, Yang Chao, Ding shuai, Lang Xinghai, Liu Hongfei, Huang Yong, Zheng Wenbao, Wang Liqiang, Gao Yiming, Feng Jun, Duan Jilin, Song Yang, Wang Yiyun, Lin Bin, Fang Xiang, Zhang Zhi and Yang Huanhuan, 2014b. Two porphyry-epithermal deposit metallogenic subseries in Tibetan Plateau: Practice of “absence prospecting” deposit metallogenic series. *Mineral Deposits* 33: 1151–1170 (in Chinese with English abstract).
- Wang Qin, Tang Juxing, Fang Xiang, Lin Bin, Song Yang, Wang Yiyun, Yang Huanhuan, Yang Chao, Li Yanbo, Wei Lujie, Feng Jun and Li Li, 2015. Petrogenetic setting of andesites in Rongna ore block, Tiegelong Cu (Au-Ag) deposit, Duolong ore concentration area, Tibet: Evidence from zircon U-Pb LA-ICP-MS dating and petrogeochemistry of andesites. *Geology in China*, (5): 1324–1336 (in Chinese with English abstract).
- Wang Sungshan, 1983. Age determinations of  $^{40}\text{Ar}/\text{Ar}$ ,  $^{40}\text{K}/\text{Ar}$  and radiogenic  $^{40}\text{Ar}$  released characteristics on K-Ar geostandards of China. *Scientia Geologica Sinica*, 4: 315–323 (in Chinese with English abstract).
- Wang Yinxi, Yang Jiedong, Chen Jun, Zhang Kaijun and Rao Wenbo, 2007. The Sr and Nd isotopic variations of the Chinese Loess Plateau during the past 7 Ma: Implications for the East Asian winter monsoon and source areas of loess. *Palaeogeography Palaeoclimatology Palaeoecology*, 249(3): 351–361.
- Xin Hongbo, Qu Xiaoming, Wang Ruijiang, Liu Hongfei, Zhao Yuanyi and Huang Wei. 2009. Geochemistry and Pb, Sr, Nd isotopic features of ore-bearing porphyries in Bangong Lake porphyry copper belt, western Tibet. *Mineral Deposits*, 28(6): 785–792.
- Yang Chao, Tang Junxing, Wang Yiyun, Yang Huanhuan, Wang Qin, Sun Xinguo, Feng Jun, Yin Xianbo, Ding Shuai, Fang Xiang, Zhang Zhi and Li Yubin, 2014. Fluid and geological characteristics researches of Southern Tiegelong epithermal porphyry Cu-Au deposit in Tibet. *Mineral Deposits*, 33: 1287–

- 1305 (in Chinese with English abstract).
- Yang Zhiming, Hou Zengqian, Song Yucai, Li Zhenqing, Xia Daixiang and Pan Fengchu. 2008. Qulong superlarge porphyry Cu deposit in Tibet: geology, alteration and mineralization. *Mineral Deposits*, 27(3): 279–240 (in Chinese with English abstract).
- Yin, A., and Harrison, T.M., 2000. Geologic evolution of the Himalayan Tibetan Orogen. *Annu. Rev. Earth Planet. Science Letter*, 28: 211–280.
- Zhang Zhi, Yao Xiaofeng, Tang, Juxing, Li Zhijun, Wang Liqiang, Yang Yi, Duan Jilin, Song Junlong and Lin Xin, 2015. Lithogeochemical, Re-Os and U-Pb geochronological, Hf-Lu and S-Pb isotope data of the Ga'erqiong-Galale Cu-Au ore-concentrated area: Evidence for the Late Cretaceous magmatism and metallogenic event in the Bangong-Nujiang suture zone, northwestern Tibet, China. *Resource Geology*, 65 (2): 76–102.
- Zhou Xiong, Fei Guangchun, Zhou Yu, Wen Chunqi, Zhang Yi and Yue Xiangyuan, 2015a. Chronology and crust-mantle mixing of ore-forming porphyry of the Bangongco: evidence from zircon U-Pb age and Hf isotopes of the Naruo porphyry copper-gold deposit. *Acta Geologica Sinica* (English Edition), 89(1): 217–228.
- Zhu Dichen, Li Shimin, Cawood, P.A., Wang Qing, Zhao Zhidan, Liu Sheng'ao and Wang Liquan, 2015a. Assembly of the Lhasa and Qiangtang terranes in central Tibet by divergent double subduction. *Lithos*. <http://dx.doi.org/10.1016/j.lithos.2015.06.023>
- Zhu Xiangping, Chen Huaan, Ma Dongfang, Huang Hanxiao, Li Guangming, Li Yubin and Li Yuchuang, 2011. Re-Os dating for the molybdenite from Bolong porphyry copper-gold deposit in Tibet, China and its geological significance. *Acta Petrologica Sinica*, 27(7): 2159–2164 (in Chinese with English abstract).
- Zhu, Xiangping, Chen Huaan, Ma Dongfang, Huang Hanxiao, Li Guangming, Li Yubin, Li Yuchang, Wei Lujie and Liu Chaoqiang, 2013.  $^{40}\text{Ar}/^{39}\text{Ar}$  dating of hydrothermal K-feldspar and hydrothermal sericite from Bolong porphyry Cu-Au deposit in Tibet. *Mineral Deposits*, 32: 954–962 (in Chinese with English abstract).
- Zhu Xiangping, Li Guangming, Chen Huaan, Ma Dongfang and Huang Hanxiao, 2015b. Zircon U-Pb, Molybdenite Re-Os and K-feldspar Ar-40/Ar-39 dating of the Bolong porphyry Cu-Au deposit, Tibet, China. *Resource Geology*, 65(2): 122–135.
- About the first author**  
LIN Bin, male, born in 1987, PhD candidate of Chinese Academy of Geological Sciences and CODES, University of Tasmania. He has taken part in the exploration and research of many large, super-large deposits, such as Jiama porphyry Cu polymetallic deposit, Zhixikang Pb-Zn-Sb-Ag deposit. Now, He is engaged in study of Mineral deposit and exploration in the Duolong area, Tibet, under the mentorship of Chen Yuchuan and David. R. Cooke. Address: No.26, Baiwanzhuang street, Xicheng District, Beijing, China (100037); Room 214, CODES, Grosvenor street, Sandy Bay, Hobart, Tasmania, Australia (7001). E-mail: bin.lin@utas.edu.au. 279865185@qq.com.